Comparison Between Two Modeling Aspects to Investigate Seismic Soil–Structure Interaction in a Jointless Bridge

S. Dhar and K. Dasgupta

Abstract Seismic waves propagate through a series of rock and soil layers before they interact with the foundation and superstructure. Besides the original characteristics of the earthquake motion at the instant of fault rupture, it is also essential how the soil site responds in terms of amplification or de-amplification for different frequency contents. A coupled soil–structure model is required to capture the dynamic behavior of the entire system efficiently, considering the possible nonlinear response of soil and structure. This paper focuses on the comparison of two modeling strategies for Soil–Structure Interaction (SSI) aiming to define the behavior of a jointless bridge, namely, (a) one with an explicit full-scale soil domain with bridge model and (b) another with Beam on Dynamic Winkler's Foundation (BDWF)/nonlinear soil springs. Finally, the structural components that affect the overall behavior of superstructure are compared between these two models, and the variation of seismic response from the performance-based study is discussed.

Keywords Beam on dynamic Winkler foundation (BDWF) · Soil continuum · Jointless bridge · Abutment–backfill interaction

1 Introduction

Creation of full-scale soil domain as continuum requires significant attention and expertise, and the analyses are numerically costly for SSI investigation. In particular, two models of a specific bridge are investigated by using a structure that resembles the well-known Humboldt Bay Middle Channel (HBMC) Bridge in California. Though, modeling the target bridge through the proper definition of all details to describe its

S. Dhar (✉) · K. Dasgupta
Indian Institute of Technology Guwahati, Guwahati, Assam 781039, India
e-mail: sdhar@ucla.edu

K. Dasgupta
e-mail: kd@iitg.ac.in

S. Dhar
University of California Los Angeles, Los Angeles, CA 90095, USA

S. Dutta et al. (eds.), *Advances in Structural Vibration*, Lecture Notes in Mechanical Engineering, https://doi.org/10.1007/978-981-15-5862-7_11

seismic response was already achieved in the past studies [1, 2] and is not the goal of the present work.

In the first approach, a full-scale soil-foundation-bridge with or without abutment–backfill interaction (i.e., *full SSI with/no BA* models) is modeled in *OpenSees* [3, 4] and the second approach, nonlinear springs are introduced to represent soil stiffness, replicating Soil–Pile Interaction (SPI) and Abutment–Backfill Interactions (ABI) (i.e., *FB_SD no/with BA* models). Hence, in the first and the second modeling approaches, different structural parameters are compared to investigate the overall response of the bridge structure. Modeling of *full SSI no/with BA* models is computationally expensive and time-consuming. Thus, modeling of continuous soil domain to consider SSI is not a very common practice in design firms, currently. So, to incorporate simplistic SSI in seismic analysis of the bridge, continuous soil domain has been replaced with nonlinear spring-dashpots to take care of SSI in *FB_SD no/with BA* models. Further, comparisons are made with and without ABI between these two modeling approaches.

2 Selection of Ground Motions

A Uniform Hazard Response Spectrum (UHRS) for bedrock-level ground motions is used as the target spectrum to select and scale the input ground motions for the analyses as discussed in Dhar et al. [5]. The UHRS is developed from the 2008 United States Geological Survey [6] national seismic hazard maps for the Humboldt Bay area for rock outcrop assuming $V_{S,\,30m} = 800$ m/s (according to NEHRP [7], site class B). The corresponding 5% damped elastic displacement response spectrum has been given as target to REXEL-Disp [8] to select the ground motions for dynamic analysis from strong ground motion database SIMBAD [9]. The input parameters in REXEL-Disp to find the ground motions are: magnitude = 5.5−7.5; fault to site distance = 0−30 km; spectrum matching tolerance = ±20%; spectrum matching period = 0.2−5 s; site specification = EC8 site class A; probability of exceedance = 10% in 50 years, representing the return period of 475 years. Seven real record ground motions are chosen for horizontal input motion by scaling their respective displacement spectra within the period of interest, such that the average displacement spectrum lies within the tolerance limits. Different parameters of selected motions are given in Table 1. The corresponding 5% damped elastic displacement spectra with the average of the ground motions are shown in Fig. 1.

Table 1 shows the set of selected and scaled rock outcrop ground motions [5]. The ground motions which are highlighted in gray are chosen to discuss in detail the soil and structural response. The Acceleration Time Histories (ATHs) of the chosen ground motions and their Fourier transform are shown in Fig. 2. The two decided ground motions (GM#1 and GM#2) correspond to the same station but with different Peak Ground Acceleration (PGA) amplitudes. Thus, the focus of this paper is to identify similarities and differences between the two different modeling techniques in the light of the observed response.

Table 1 Different parameters of selected ground motions [5]

Station ID	Earthquake name	Date	M_w	Epicentral distance, km	PGA, m/s^2	Scaled PGA, m/s^2
ALT	Irpinia	November 23, 1980	6.9	23.77	0.54	3.46
ST_106	South Iceland	June 17 2000	6.5	5.25	3.39	3.06
ST_112	Olfus	May 29, 2008	6.3	8.25	3.28	5.47
ST_101	Olfus	May 29, 2008	6.3	7.97	5.00	7.06
BSC	Irpinia	November 23, 1980	6.9	28.29	0.95	0.68
ST_106	South Iceland	June 21, 2000	6.4	21.96	0.51	0.73
LPCC	Christchurch	February 21, 2011	6.2	1.48	9.16	12.64
Mean values:			6.5	13.85	3.26	4.73

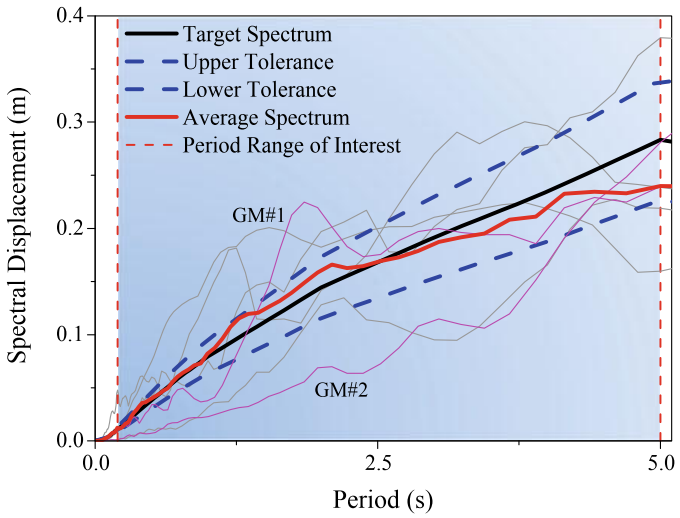

Fig. 1 Displacement spectra of all the ground motions used in the present study; the period of interest is shown within a blue shadow. Chosen ground motions for discussing the results are also marked

3 Modeling

3.1 Structural Modeling

As illustrated in detail in Zhang et al. [1], the Humboldt Bay Middle Channel Bridge, located near Eureka in California (USA), is 330 m long, 10 m wide, and 12 m high (average height over mean water level). The bridge superstructure consists of nine spans with four precast prestressed concrete I-girders and cast-in-place concrete

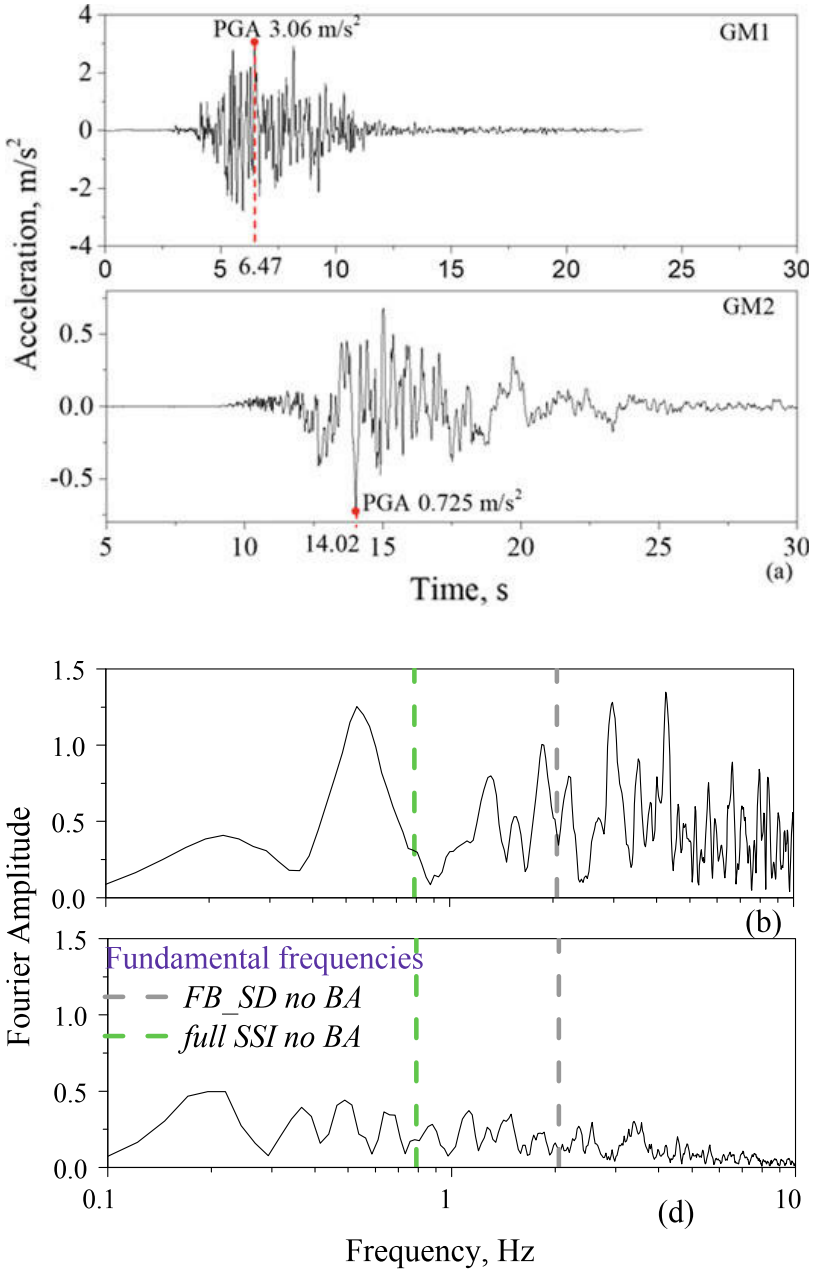

Fig. 2 Rock outcrop earthquake (scaled) records used in this study: **a** strike-slip fault of the June 17, 2000 South Iceland Earthquake; Ground Motion (GM) #1, **b** Fourier amplitude spectrum of GM#1, **c** strike-slip fault of the June 21, 2000 South Iceland Earthquake; Ground Motion (GM) #2, and **d** Fourier amplitude spectrum of GM#2 with the fundamental frequency (marked) for different considered models

slabs. The bridge deck is resting on two integral abutments monolithically connected with continuous deck, and the shear keys are exempted at the superstructural level, to serve the purpose of our present study which is to investigate the behavior of an integral bridge [10]. Pile caps of 1 m thickness are supported by deep foundations consisting of driven precast prestressed concrete pile groups. For the sake of simplicity, only the longitudinal dynamic response is analyzed in this study. Two finite element models of the bridge are considered: a linear model with elastic beam-column elements for both the superstructure and substructure (piers) and a nonlinear model where piers are modeled using force-based fiber elements. The elastic properties of structural elements are adapted from Zhang et al. [1] as A (area, m^2) = 12, 4.56, 3.4 and I (moment of inertia, m^4) = 1.44, 3.212, 0.8188 for abutment, deck and pier sections, respectively. All the concrete elements have the same elastic modulus of 28 GPa. The details of the pile group modeling have been discussed in Dhar et al. [11].

In the nonlinear simulations, force-based fiber elements [12] with five integration points are used in piers. Pier cross section is discretized as shown in Fig. 3a. Kent-Park-Scott [13] concrete model is used to model nonlinear concrete material with degraded linear unloading/reloading stiffness, and no tensile strength is considered. Giuffre-Menegotto-Pinto [14] steel material is specified with 0.8% isotropic strain hardening for reinforcement bars with 200 GPa elastic modulus and 276 MPa yield strength. The properties of confined and unconfined concrete used in the study are the same as those adopted by Zhang et al. [1]. Compressive strengths of confined and unconfined concrete are 34.5 MPa and 27.6 MPa, respectively. The simulations have been performed using the finite element program *OpenSees* [4]. Rayleigh damping scheme is introduced as viscous material damping to calibrate the Rayleigh damping parameters. The damping ratio is prescribed as 5% at 0.5 Hz and 5.0 Hz for *full SSI no/with BA* models in *OpenSees* shown in Fig. 3b.

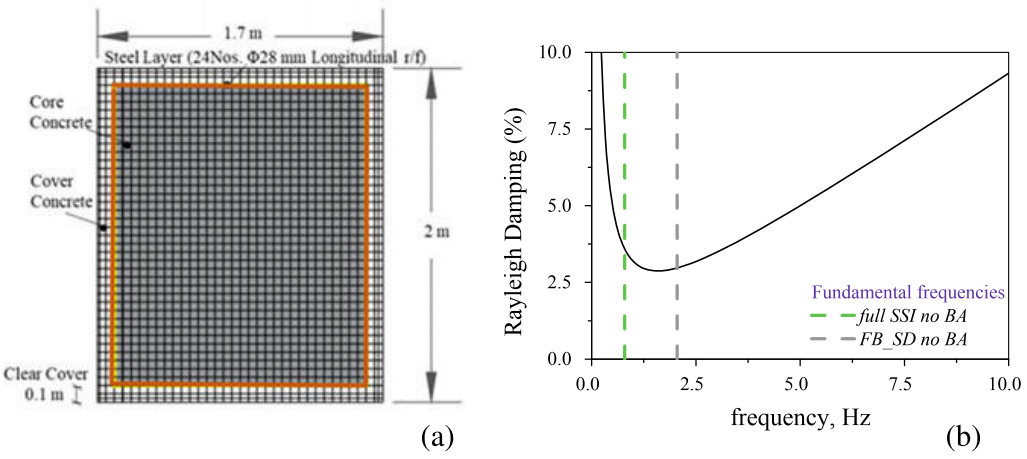

Fig. 3 **a** Fiber-based discretization of the pier cross section with reinforcement and **b** Rayleigh damping considered for the SSI analyses

3.2 Geotechnical Modeling

Two-dimensional soil modeling has been carried out in *OpenSees*. Soil domain is 1500 m wide (evaluated through iterations to reach free-field motion at the boundary) and 220 m in depth. The entire soil domain consists of 4 different layers (Fig. 4a) having the static and dynamic properties (Table 2), in which the geotechnical constitutive parameters are adapted from Zhang et al. [1]. Pressure independent multi-yield material has been used to describe the soil behavior through a formulation based on the multi-surface plasticity concept [15] with associative flow rule, inbuilt in *OpenSees*. The yield surfaces are of the Von Mises type. Since total stress analyses

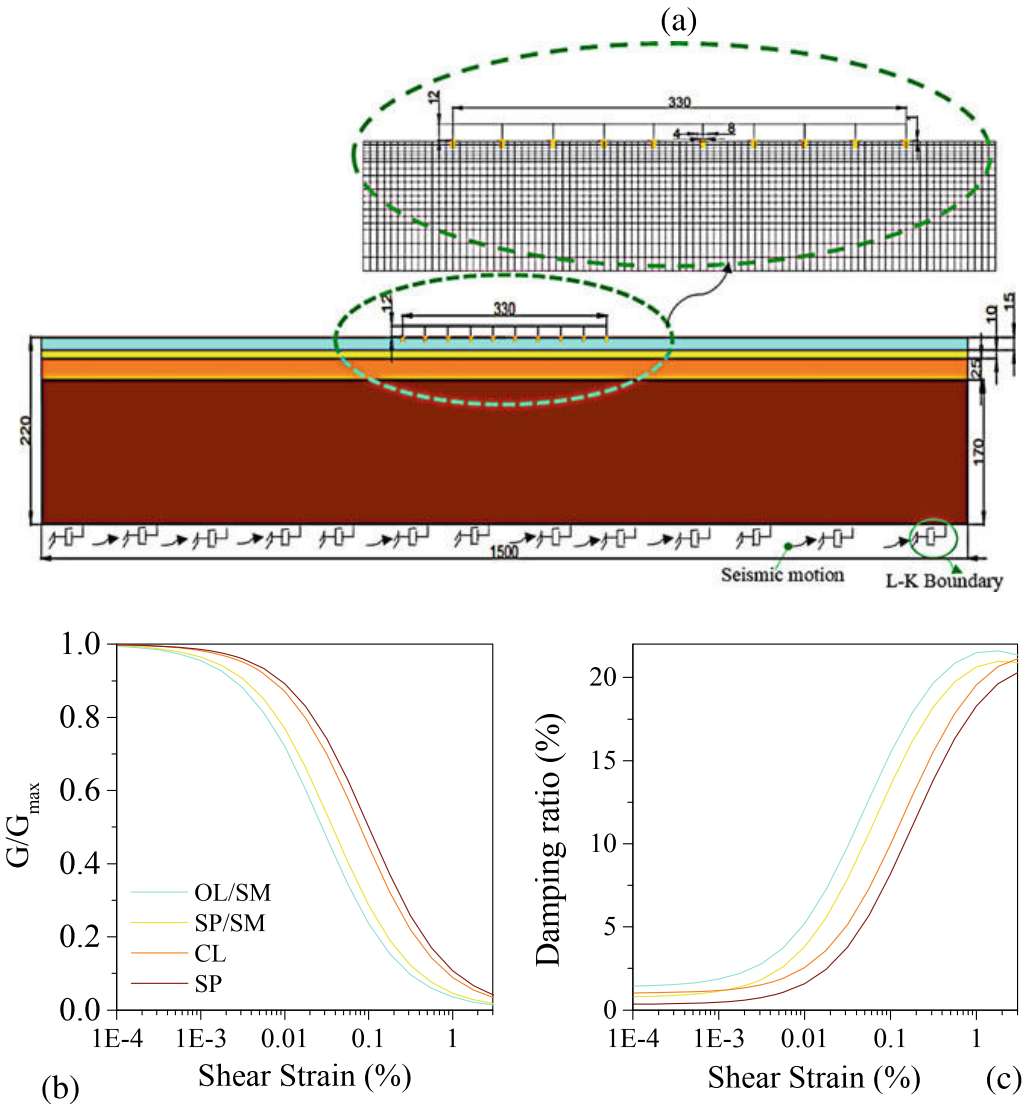

Fig. 4 **a** *Full SSI no BA* model in OpenSees (all dimensions in m), **b** Normalized shear modulus degradation versus shear strain and **c** Damping ratio versus shear–strain curves for different soil layers (Darendeli 2001). Explicit details of the numerical modeling are provided in [11]

Table 2 Properties of different soil layers used in the present study (modified after [1])

Soil layer	Elastic properties			Nonlinear properties		
	Maximum shear modulus (MPa)	Poisson's ratio	Total unit weight (t/m^3)	Undrained shear strength, (kPa)	Shear modulus ratio (Fig. 4b, c)	Plasticity Index
OL/SM	76	0.45	1.9	30	Cyan Line	10
SP/SM	171	0.45	1.9	11.9	Yellow Line	0
CL	288	0.45	1.8	100	Orange Line	30
SP	525	0.45	2.1	52.5	Brown Line	0

are carried out, any direct consequence of significant excess pore water pressure generation is naturally neglected in the present study. To represent the nonlinear nature of the soil domain, variation of shear modulus degradation and damping ratio with shear strain are adapted as per the proposition of Darendeli [16], shown in Fig. 4b, c, respectively. The soil domain lateral boundary conditions are implemented by Tied Degrees of Freedom (TDOF) [2, 17] at the lateral two ends of the soil domain. Thus, the soil domain follows the pattern of a 2D shear beam constraints, in which generally the horizontal response dominates over the vertical response. At the base level, classical Lysmer and Kuhlemeyer [18] type absorbing boundary conditions are applied in the horizontal direction by adequately calibrating the dashpot coefficients together with the classical vertical displacement restraints. The dynamic base input motion is given in horizontal direction to study the horizontal response of the soil–structure system. In the case of *full SSI no/with BA* models, the precast prestressed concrete pile groups, considered linear elastic in all the analysis, are analyzed per [19−21] with an equivalent pile group of stiffness 1.1 GPa. The precast driven piles are of 5.2 m in length and floating type. In the case of *full SSI with BA* model (Fig. 5), abutment–backfill dynamic properties are kept similar to the soft clayey soil (topmost layer) of the soil domain. The effects of gaps or interfaces are excluded at the abutment–backfill interface.

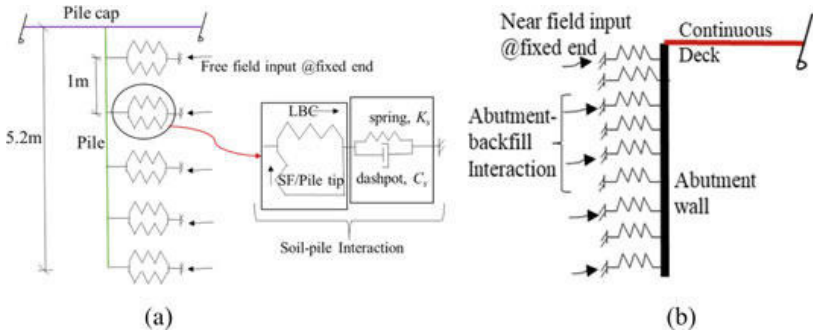

Fig. 5 Schematic diagram of **a** soil–pile interaction and **b** abutment–backfill interaction modeled in the present study (adapted from [11])

In the simplified models, on the other hand, *FB_SD no BA* model represents the Soil–Pile Interaction (SPI), and *FB_SD with BA* serves SPI and ABI, together. In the models above, SPI and ABI are represented through classical nonlinear two-noded zero-length links and dashpots to represent idealized SSI at far and near fields. In the near field spring-dashpot system, hysteretic damping is considered through nonlinearity of multi-linear plastic uniaxial material, inbuilt in *OpenSees*. Lateral and vertical springs are modeled as per API-rp2a [22] in parallel to represent lateral load-bearing capacity and skin friction of pile shaft or pile tip end bearing, respectively. Far-field soil stiffness and radiation damping are modeled using the coefficients provided by Gazetas and Dobry [23]. Far-field spring-dashpots are linear elastic and modeled in series with near-field hysteretic springs. Far-field spring and dashpots are modeled in a parallel configuration. At the fixed end of far-field spring-dashpots, free-field motions are applied based on the exact depth of soil column at the corresponding depth of springs. Detailing of springs and dashpots with the schematic diagrams of SPI (modeled explicitly with near-field and far-field) and ABI are discussed in Fig. 5a, b, respectively; where K_s is the linear stiffness, C_s is the radiation dashpot coefficient of far-field spring and SF for skin friction of pile. It was proved in past researches [24−26] that force–displacement relationships from API overestimate the soil stiffness to address SPI. Therefore, the implementation of API curves in *FB_SD no/with BA* models gives a conservative response. Moreover, far-field spring-dashpots are linear elastic. Thus, to reduce this error, 10% Rayleigh damping is introduced in *FB_SD no/with BA* models.

In *FB_SD with BA* model, nonlinear springs are added to model abutment–backfill soil. The abutment is considered as frame-type abutment, and nonlinear springs are positioned at 1 m distance along with the height of abutment (Fig. 5b). The force–deformation curves for the springs are calculated as per the Highway Agency [27].

4 Analysis

During the first phase of the study, two models are compared, namely, (a) *full SSI no BA model* and (b) *FB_SD no BA* model. Initially, a single-step static analysis is carried out. Then, input motion is applied as force–time history at the base of the soil domain in *full SSI with BA* model. For *FB_SD with BA* model, after static gravity analysis, free-field input motions are applied at different corresponding depths as Displacement Time Histories (DTHs) extracted from 2D ground response analysis of similar soil column performed in *OpenSees*. For *full SSI with BA* and *FB_SD with BA* models, salient parameters are compared in the following sections, and differences in structural behavior from nonlinear THA are discussed.

5 Results

5.1 Comparison of the Response of Full SSI no BA and FB_SD no BA Models

From Fig. 6a, b under GM#1, eighth pier top and bottom ATHs are compared and in (c) and (d) their respective Fourier Transforms (FT) are shown. The observed ATHs at the bottom of the pier have similar values (Fig. 6a, c), but at the deck level (Fig. 6b, d) *FB_SD no BA* model shows a more amplified response as compared to the *full SSI no BA* model. However, the peaks of Fourier amplitude occur at 1.78 Hz and 2.29 Hz for *FB_SD no BA* and *full SSI no BA* models, respectively. Foundation of *FB_SD no BA* model is found to be stiffer and nonlinearity still not developed in the underlying soil because the API curves overestimate soil stiffness at different depths of piles. Moreover, a resonance effect is also noted near 2 Hz, which is not present in the fully coupled SSI counterpart.

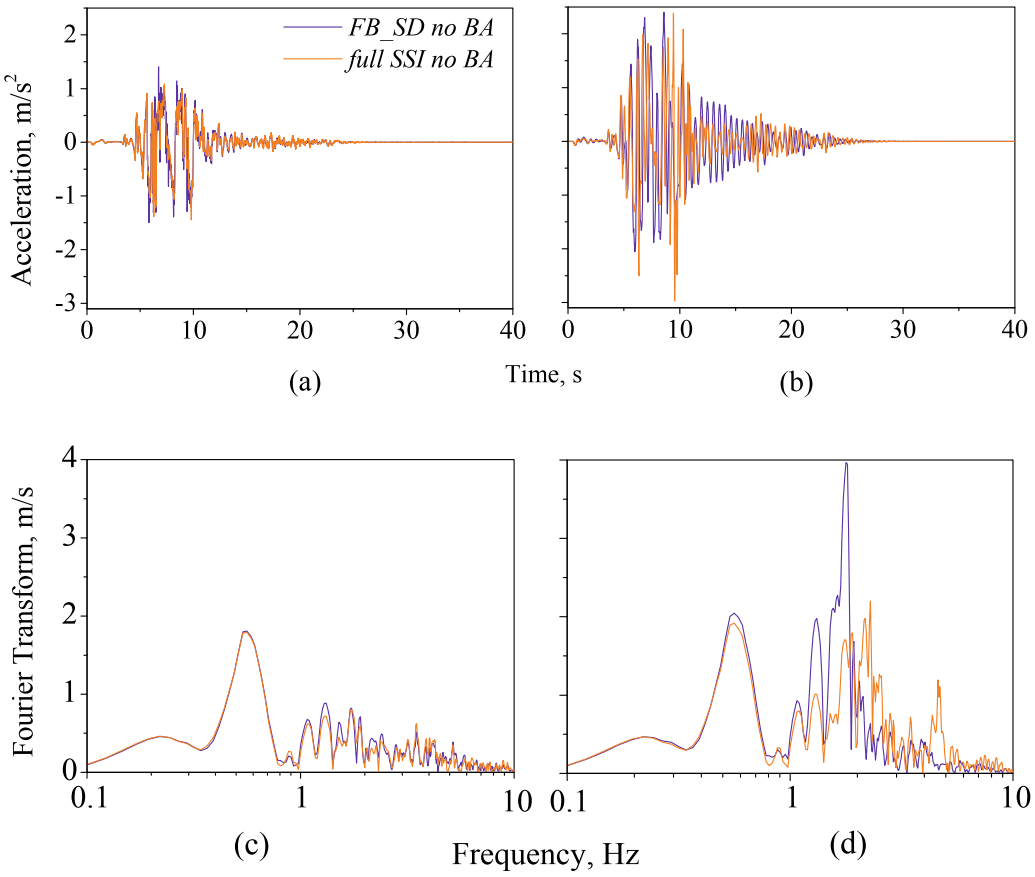

Fig. 6 Acceleration time history (ATH) **a** at the bottom, **b** ATH at the top of eighth pier, **c** FT of the ATH shown at (**a**) and (**d**) FT of the ATH in (**b**) under GM#1

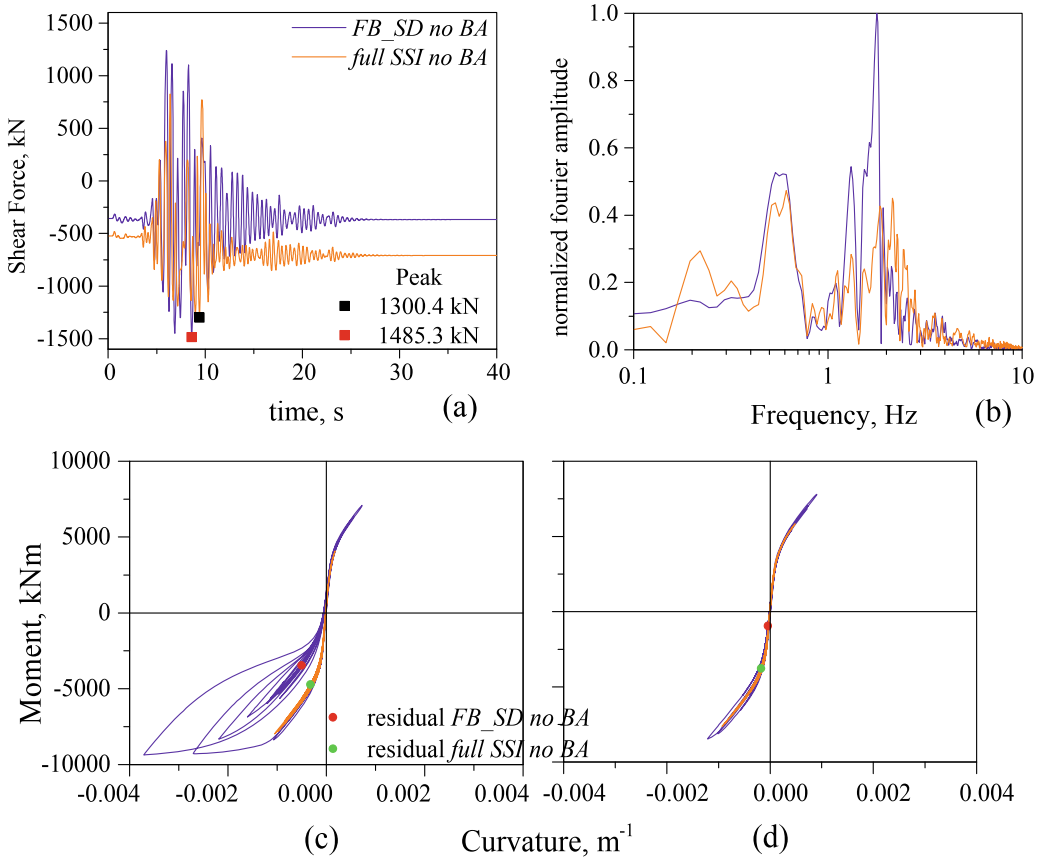

Fig. 7 **a** Shear force time history at the top of eighth pier and **b** Fourier transform of the SFTH. Moment curvature response of eighth pier at **c** top and **d** bottom under GM#1

A similar response is observed for Shear Force Time History (SFTH) plots in Fig. 7a. Due to seismic waves amplification at the deck level, SFTH is higher in *FB_SD no BA* model. From the SFTH, it can be stated that *FB_SD no BA* model shows significantly less nonlinearity in the bridge substructure component as compared to the *full SSI no BA* model. From normalized FT of SFTHs in Fig. 7b, it is observed that the peak of the Fourier amplitude of *FB_SD no BA* model is at 1.78 Hz, thus the magnitude of Fourier amplitude is significantly higher. This implies that once the seismic waves propagate from the foundation to the deck level, *FB_SD no BA* model shows a more amplified response as compared to the *full SSI no BA* model. This is also evident from the moment–curvature response at the top and bottom sections of the eighth pier (Fig. 7c, d). Moment–curvature response at the top of the eigth pier is found to be underdamped in *FB_SD no BA* model and mainly forms the negative moment–curvature loops in the third quadrant. At the base of the eighth pier, moment–curvature response (Fig. 7d) shows a similar pattern on the opposite quadrants. After investigating several parameters at the top and base of the pier, it can be stated that *FB_SD no BA* model is getting more amplified from the foundation to the deck level as compared to the *full SSI no BA* model; thus, mismatches in response arise for different response parameters at the deck level.

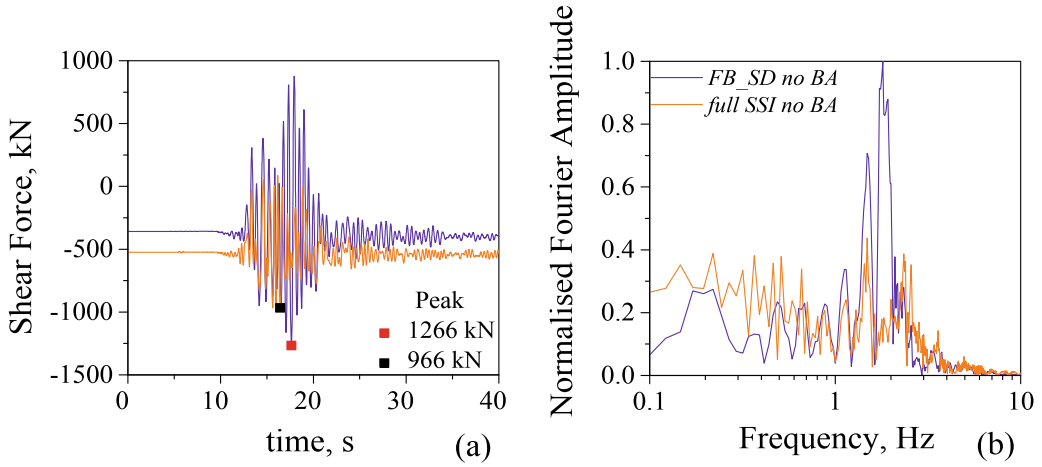

Fig. 8 **a** SFTH at the top of eighth pier and **b** FT of the SFTHs in (**a**)

Under GM#2, SFTHs at the top of the eighth pier (deck level) are shown for the two models in Fig. 8a. The difference in the energy content of the response is observed through the normalized FT of SFTHs in Fig. 8b.

5.2 *Comparison of the Response of Full SSI with BA and FB_SD with BA Models*

For comparison, the ATHs are shown at the top and the bottom of the eighth pier in Fig. 9a, b, and the corresponding Fourier amplitudes of ATHs are shown in Fig. 9c, d under GM#1. ATH at the base of the pier in *FB_SD with BA* model is marginally higher than *full SSI with BA* model. Thus, in Fig. 9c, the peaks of the amplitudes are higher from 0.6 Hz onwards. However, at the top of the eighth pier (Fig. 9b) ATHs are quite comparable for both the models. In Fig. 9d, peak Fourier amplitudes for *FB_SD with BA* and *full SSI with BA* models are at 2.83 Hz and 2.12 Hz, respectively, which indicate that *FB_SD with BA* model is marginally stiffer as compared to the *full SSI with BA* model.

Under GM#2, similar responses are observed, at the top and bottom of first pier ATHs in Fig. 10a, b and their corresponding FTs in Fig. 10c, d, respectively. Due to low-intensity input motion, the ATHs at the base of the pier are quite similar for both the models along with their FTs. At the top of the pier, ATHs have two different peaks at different time instants. In Fig. 10d, peak amplitudes occur at the frequencies of 1.48 Hz and 3.07 Hz for *FB_SD with BA* and *full SSI with BA* model, respectively. At the low intensity of PGA input, foundation soil is expected to behave in the linear elastic range. As the nonlinearity of the foundation soil does not influence the behavior of the superstructure, the bridge is observed to be more flexible for *FB_SD with BA* model as compared to the *full SSI with BA* model. Thus, the peak of FT at

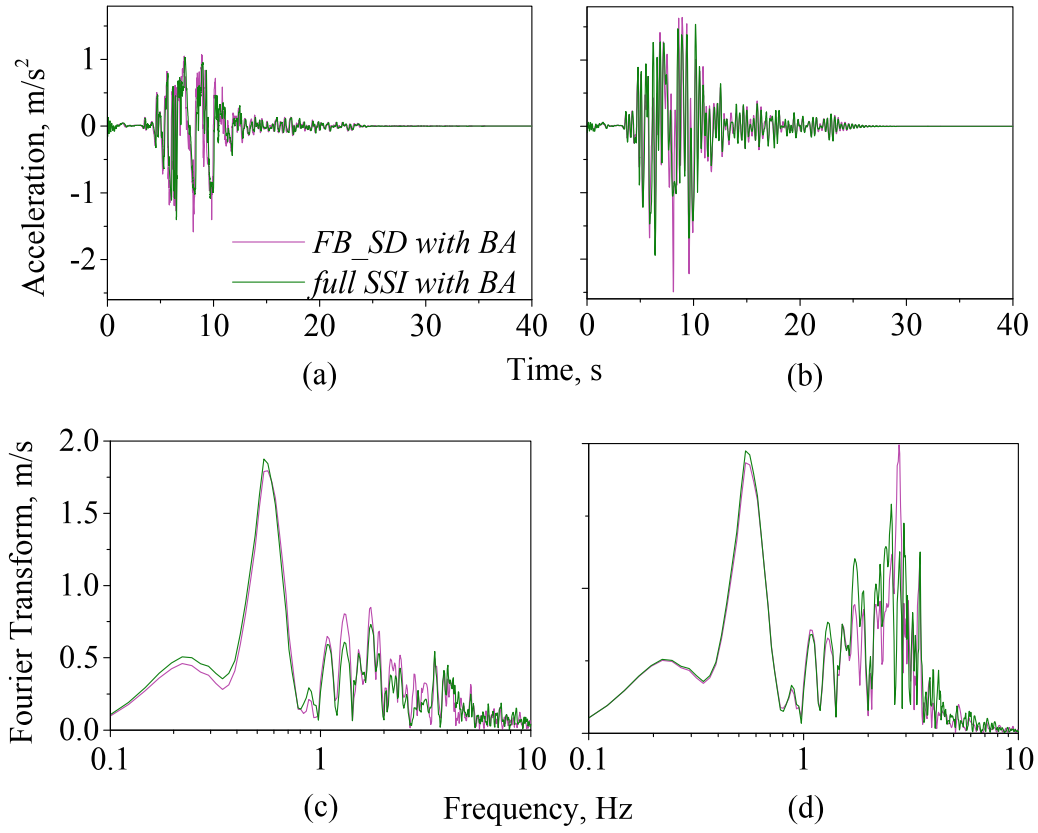

Fig. 9 ATH **a** at the top and **b** at the bottom of eighth pier, **c** Fourier transform of the ATH shown in (**a**) and (**d**) Fourier transform of the ATH in **b** under GM#1

deck level in *FB_SD with BA* model is at lower frequency instant than *full SSI with BA* model. Moreover, amplitudes are quite the same both spectrally and temporally.

At the top of the eighth pier of *FB_SD with BA* model in Fig. 11a under GM#1, both the peak and the residual shear forces are higher as compared to the *full SSI with BA* model; this shows that more nonlinearity develops in the *FB_SD with BA* model under GM#1. The Fourier amplitude plot of SFTHs in Fig. 11b shows that in *FB_SD with BA* model, the seismic forces are higher as compared to the *full SSI with BA* model with a frequency of 0.8 Hz, beyond which the SSI model shows higher seismic force. The peaks of Fourier amplitudes occur at 0.42 Hz and 1.06 Hz for *FB_SD with BA* and *full SSI with BA* models, respectively. Thus, it signifies that in the former model, the seismic response is being more amplified at deck level and more nonlinearity develops at pier sections than the *full SSI with BA* model. Under GM#2, the variation of SFTHs at the top of the eighth pier shows that the peak shear force in *FB_SD with BA* model is higher than the *full SSI with BA* model (Fig. 11c); also the *FB_SD with BA* model shows a higher residual response. Thus, in *FB_SD with BA* model piers have developed significant nonlinearity as compared to the *full SSI with BA* model. From the comparison of Fourier amplitudes of SFTHs in Fig. 11d, the seismic force content is observed to be higher in *FB_SD with BA* model up to a frequency of 1 Hz, beyond which the *full SSI with BA* model carried higher forces

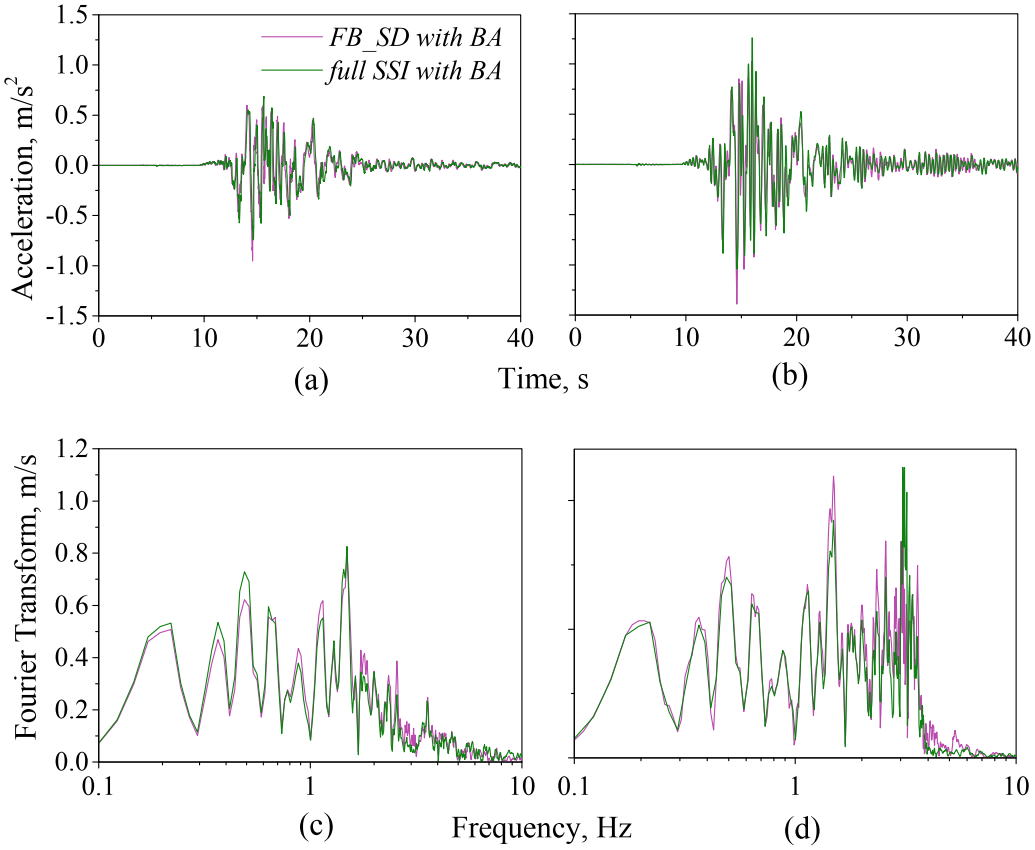

Fig. 10 ATH **a** at the top, **b** ATH at the bottom of first pier, **c** Fourier transform of the ATH shown at (**a**) and (**d**) Fourier transform of the ATH in (**b**) under GM#2

in the high-frequency range. Thus, the *FB_SD with BA* model is weaker and more flexible than *full SSI with BA* model.

6 Conclusion

Based on the nonlinear time history analysis of the bridge-soil system under the two selected ground motions, the two mentioned modeling approaches yield reasonably close response. The salient conclusions are stated as follows:

- As compared to the *full SSI no/with BA* models, shear forces and bending moments at piers are higher for *FB_SD with/no BA* models because foundation soil stiffness is more elevated in API force–displacement curves for clayey soil.
- The *full SSI with BA* model is observed to show the lowest nonlinear dynamic response for the bridge structure. As the backfill soil provides longitudinal restraints to the bridge, the seismic force from the superstructure dissipates into the backfill soil through passive resistance.

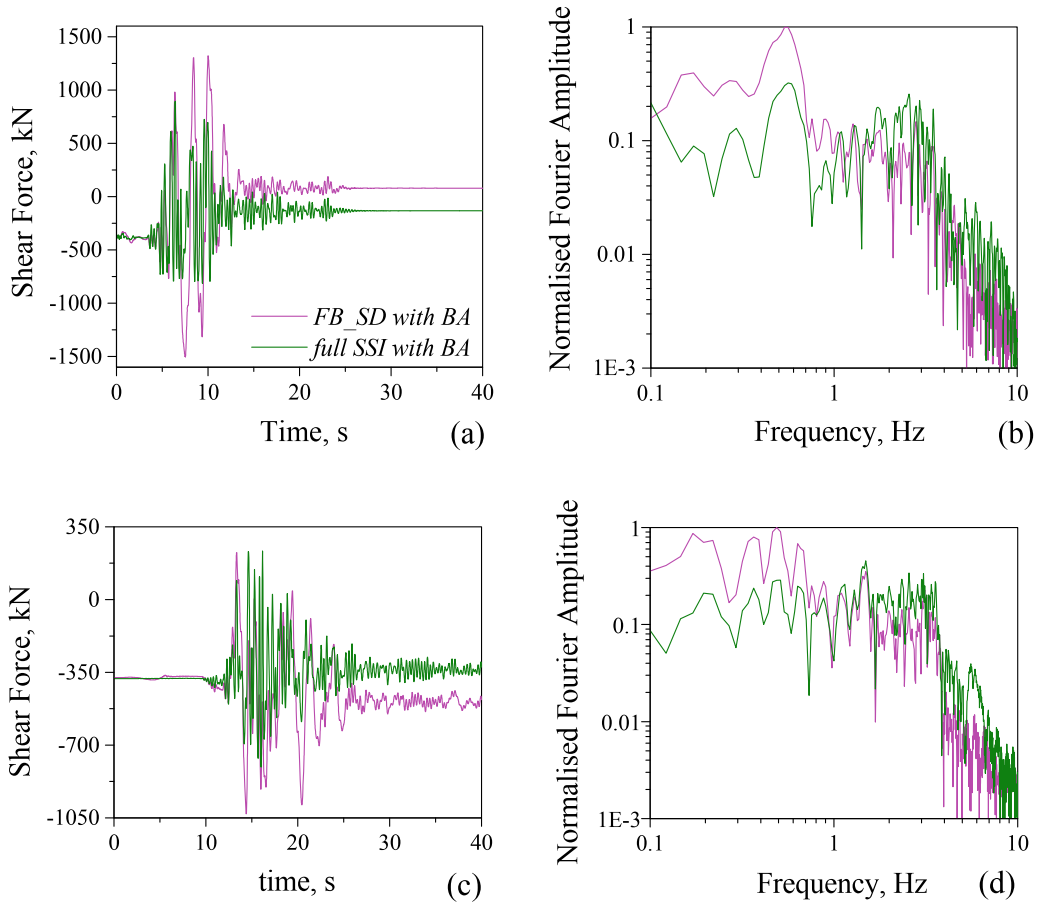

Fig. 11 **a** SFTHs at the top of eighth pier and **b** Fourier transform of the SFTHs in (a) under GM#1, (c) SFTHs at the top of eighth pier and **d** Fourier transform of the SFTHs in **c** under GM#2

- *FB_SD no BA* model shows a higher response as compared to the *full SSI no BA* model as the prescribed API guidelines overestimate the soil stiffness for the foundation soil. The structural response is amplified significantly at the deck level for *FB_SD no BA* model and results in higher forces and moments at pier–deck junctions.
- For *FB_SD with BA* and *full SSI with BA* models, the former model is stiffer at superstructure level and deforms in higher curvature after dynamic analysis; thus, the mobilized nonlinearity and the residual response are observed to be higher for this modeling approach. Due to insufficient soil nonlinearity at the foundation and backfill components, the *FB_SD with/no BA* models exhibit overall higher stiffness.
- In *full SSI with/no BA* models, due to significant soil nonlinearity, bridge response does not amplify at deck level, thus in this type of modeling bridge response is lower than the simplified SSI modeling approach.

A more complete and detailed discussion of the problem has been provided in [11] for more transparent representation.

Acknowledgments Part of this research was carried out while the first author (SD) was visiting Politecnico di Milano, Italy under INTERWEAVE Project, Erasmus Mundus Program during 2014−2017. The first author would like to thank Dr. Ali Gunay Ozcebe, Prof. Roberto Paolucci, and Prof. Lorenza Petrini from PoliMi for their valuable comments during the work and Ministry of Human Resource and Development (MHRD) for the scholarship during her Ph.D.

References

1. Zhang Y, Conte JP, Yang Z, Elgamal A, Bielak J, Acero G (2008) Two dimensional nonlinear earthquake response analysis of a bridge-foundation ground system. Earthq Spectra 24(2):343–386
2. Elgamal A, Yan L, Yang Z, Conte JP (2008) Three-dimensional seismic response of Humboldt bay bridge-foundation-ground system. Jr Struct Eng ASCE 134(7):1165–1176
3. Mazzoni S, McKenna F, Scott HM, Fenves GL (2007) The OpenSees command language manual. v6.0 http://opensees.berkeley.edu, PEER, University of California, Berkeley
4. McKenna F, Fenves GL (2008) Using the OpenSees interpreter in parallel computers. University of California, Berkeley. NEESit; TN-2007-16, v1.0
5. Dhar S, Özcebe AG, Dasgupta K, Dey A, Paolucci R, Petrini L (2016) Nonlinear dynamic soil-structure interaction effects on the seismic response of a pile-supported integral bridge structure. In: 6th international conference on recent advances in geotechnical earthquake engineering and soil dynamics. Paper No. 141, India
6. Petersen MD, Frankel AD, Harmsen SC, Mueller CS, Haller KM, Wheeler RL, Wesson RL, Zeng Y, Boyd OS, Perkins DM, Luco N, Field EH, Wills CJ, Rukstales KS (2008) Documentation for the 2008 update of the United States National Seismic Hazard Maps. USGS Open-File Report -1128
7. Holzer TL, Padovani AC, Bennett MJ, Noce ET, Tinsley JC (2005) Mapping NEHRP VS30 site classes. Earthq Spectra 21(2):1–18
8. Smerzini C, Paolucci R, Galasso C, Iervolino I (2012) Engineering ground motion selection based on displacement-spectrum compatibility. In: Proceedings of the 15th WCEE, Paper no. 2354, Portugal
9. Smerzini C, Galasso C, Iervolino I, Paolucci R (2014) Ground motion record selection based on broadband spectral compatibility. Earthq Spectra 30(4):1427–1448
10. Dhar S, Dasgupta K (2019) Seismic soil structure interaction for integral abutment bridges: a review. Infrastruct Geotech, Transp. https://doi.org/10.1007/s40515-019-00081-y
11. Dhar S, Özcebe AG, Dasgupta K, Paolucci R, Petrini L (2019) Different approaches for numerical modeling of seismic soil-structure interaction: impacts on impacts on the seismic response of a simplified reinforced concrete integral bridge. Eq Struct 17(4):373–385.https://doi.org/10.12989/EAS.2019.17.4.373
12. Neuenhofer A, Filippou FC (1998) Geometrically nonlinear flexibility-based frame finite element. J Struct Eng 124(6):704–711
13. Scott BD, Park R, Priestley MJN (1982) Stress-strain behavior of concrete confined by overlapping hoops at low and high strain rates. J Am Conc Ins 79:13–27
14. Filippou FC, Popov EP, Bertero VV (1983) Effects of bond deterioration on hysteretic behavior of reinforced concrete joints. Report EERC 83–19 University of California, Berkeley
15. Prevost JH (1985) A simple plasticity theory for frictional cohesionless soils. Soil Dyn Eq Eng 4(1):9–17
16. Darendeli MB (2001) Development of a new family of normalized modulus reduction and material damping curves. Dissertation, University of Texas. Austin, TX
17. Kontoe S, Zdravković L, Potts DM, Salandy NE (2007) The domain reduction method as an advanced boundary condition. In: 4th International Conference on Earthquake Geotechnical Engineering. Paper No. 1231. Greece

18. Lysmer J, Kuhlemeyer RL (1969) Finite dynamic model for infinite media. J Eng Mech Div 95(EM4):859–877
19. Ariyarathne P, Liyanapathirana DS, Leo CJ (2013) Comparison of different two-dimensional idealizations for a geosynthetic-reinforced pile-supported embankment. Int J Geomech 13(6):754–768
20. Mokwa RL (1999) Investigation of the resistance of pile caps to lateral spreading. Dissertation, Dept. of Civil Engineering, Virginia Polytechnic Institute and State University, VA
21. AASHTO LRFD (2012) Bridge Design Specifications. American Association of State Highway and Transportation Officials; Washington DC
22. API RP2A-WSD (2003) Recommended practice for planning, designing and constructing fixed offshore platforms-working stress design. Am. Petrol. Ins. Washington DC
23. Gazetas G, Dobry R (1984) Horizontal response of piles in layered soil. J Geotech Eng Div 110(1):20–40
24. Granas JL (2016) Undrained lateral soil response of offshore monopile in layered soil. M.Tech Thesis Dept. of Civ. & Transport. Eng. NTNU
25. Brødbæk KT, Møller M, Sørensen SPH, Augustesen AH (2009) Review of p-y relationships in cohesionless soil. DCE Technical Reports No. 57, Dept. of Civ. Eng., Aalborg University
26. Monkul MM (2008) Validation of practice oriented models and influence of soil stiffness on lateral pile response due to kinematic loading. Marine Geores Geotech 26(3):145–159
27. Highway Agency BA 42/96 (2003) Amendment No. 1, highway structures: Approved procedures and general design. Sec. 3.5. The Stationary Office, London